PROCEEDINGS OF SCIENCE

Electromagnetic conductivity of quark-gluon plasma at finite baryon chemical potential and electromagnetic field

G. Almirante,[a] **N. Astrakhantsev,**[b,c] **V. Braguta,**[d] **M. D'Elia,**[e,f] **L. Maio,**[e,f] **M. Naviglio,**[e,f,*] **F. Sanfilippo**[g] **and A. Trunin**

[a] *Université Paris-Saclay, CNRS/IN2P3, IJCLab, 91405 Orsay, France*
[b] *Physik-Institut, Universität Zürich, Winterthurerstrasse 190, CH-8057 Zürich, Switzerland*
[c] *Institute for Theoretical and Experimental Physics NRC "Kurchatov Institute", Moscow, 117218 Russia*
[d] *Bogoliubov Laboratory of Theoretical Physics, Joint Institute for Nuclear Research, Dubna, 141980 Russia*
[e] *Dipartimento di Fisica dell'Universita' di Pisa, Largo B. Pontecorvo 3, I-56127 Pisa, Italy*
[f] *INFN, Sezione di Pisa, Largo B. Pontecorvo 3, I-56127 Pisa, Italy*

E-mail: manuel.naviglio@phd.unipi.it

An important aspect in the study of quark gluon matter is represented by the computation of its transport coefficients. Indeed, they contain important information about thermodynamics and the phase diagram of QCD. Furthermore, they are used as input parameters in hydrodynamical simulations of heavy-ion collision experiments. The electric conductivity is a transport coefficient which parameterizes the charge transport phenomena. It is expected to play a central role in the dynamics of the Quark Gluon Plasma (QGP), since electric and magnetic fields are generated in heavy-ion collisions. The computation of this quantity can be done using the so-called Kubo formulas where spectral functions of electric current-current correlation functions and conductivity are directly related. The spectral functions can be extracted from the correlators on the lattice. The two quantities are related by an integral relation which has to be inverted to extract spectral functions. This inversion can be done by using smearing techniques to look for approximate solutions. We performed the study of the conductivity in two cases. On the one hand, we present the lattice QCD study of the electromagnetic conductivity dependence on baryon density. A first discussion can be found in [1]. On the other hand, we studied the electromagnetic conductivity in presence of strong magnetic fields, namely $eB = 4, 9\ GeV$. This gives an evidence of the CME.

The 39th International Symposium on Lattice Field Theory,
8th-13th August, 2022,
Rheinische Friedrich-Wilhelms-Universität Bonn, Bonn, Germany

* Speaker

PoS(LATTICE2022)155

1. Introduction

Transport coefficients of quark-gluon matter contain important information about thermodynamics and the phase diagram of quantum chromodynamics (QCD). Furthermore, they are used as input parameters in hydrodynamical simulations of heavy-ion collision experiments. In particular, the electromagnetic conductivity $\sigma_{\rm el}$ is a transport coefficient which parameterizes the charge transport phenomena. The electric and magnetic fields generated in heavy-ion collisions can reach rather large values $eB \sim eE \sim m_\pi^2$ for a short period of time [2]. For this reason, charge transport is expected to play an important role in the dynamics of the fireball created by the colliding nuclei. Notice also that the quark-gluon plasma (QGP) electromagnetic conductivity can be accessed in heavy-ion collision experiments through the dilepton emission rate [3].
The QGP electromagnetic conductivity was studied using different approaches: NJL-like models [4–9], perturbative calculations [10–12], dynamical quasiparticle approach [13, 14], hadron resonance gas models [15–17] and holographic QCD [18, 19]. In addition to phenomenological studies, first-principle results on this observable were obtained within lattice simulation of QCD [20–25] (see also the review of lattice results [26]).
In general, transport coefficients of a medium can be extracted from the low-energy behaviour of appropriate current-current spectral functions. Here, an inverse problem appears. Indeed, spectral functions are related via a convolution relation to the corresponding correlation functions.
In this work, we present our lattice study of the conductivity of the quark-gluon plasma in different conditions within real QCD, considering in particular the theory with $N_f = 2 + 1$ dynamical quarks at the physical point. The study of the conductivity on the lattice consists of three main steps. The first one is the computation of the current-current correlation functions on the lattice. Then, the extraction of the spectral function from the correlators using inversion methods [27] and finally the computation of the values of the conductivity via the so-called Kubo formulas. In this work, we present how the electromagnetic conductivity is influenced by non zero baryon density, as already discussed in [1] and by the presence of strong magnetic fields.

2. Lattice setup

We consider a QCD with $N_f = 2 + 1$ flavours. The discretized partition function is

$$\mathcal{Z}(T, \mu_{u,d,s}) = \int \mathcal{D}U e^{-S_{\rm YM}} \prod_{f=u,d,s} \det \left[M_{\rm st}^f(U, \mu_f) \right]^{1/4}$$

where

$$S_{\rm YM} = -\frac{\beta}{3} \sum_{x,\mu\neq\nu} \left(\frac{5}{6} W_{x;\mu\nu}^{1\times1} - \frac{1}{12} W_{x;\mu\nu}^{1\times2} \right) \tag{1}$$

is the Symanzik tree-level improved lattice gauge action [28], and $(D_{st}^f)_{nm}$ is the stout improved rooted staggered Dirac operator that we will define separately in the following paragraphs for the case at finite baryon density and the case in presence of magnetic field. In Eq. (1), β is the inverse gauge coupling, $W^{1\times n}$s represent the real part of the traces of the ordered products of the link variables placed respectively on the 1×1 and 1×2 rectangular closed paths, starting at the lattice point x and laying on the plane $\mu\nu$.

3. Euclidean correlators and conductivity

The relevant quantities that we compute on the Lattice are the current-current lattice Euclidean temporal correlation function, namely

$$C_{ij}(\tau) = \frac{1}{L_s^3} \langle J_i(\tau) J_j(0) \rangle, \tag{2}$$

where i and j are referred to the spatial dimensions, τ is the Euclidean time, L_s the spatial extension. In this work, $J_i(\tau)$ is the i-th component of the conserved electromagnetic current. In the framework of staggered

fermions it reads

$$J_i(\tau) = \frac{e}{4}\sum_f q_f \sum_{\vec{x}} \eta_{x;i}\left(\bar{\chi}^f_x U^{(2)}_{x,i}\chi^f_{x+i} + \bar{\chi}^f_{x+i} U^{(2)\dagger}_{x,i}\chi^f_x\right), \tag{3}$$

where $e^2 = 4\pi/(137.04)$ is the elementary charge, q_f is the electric charge of the quarks, $\vec{x} = (\tau, \vec{x})$, $i = 1, 2, 3$, and $\bar{\chi}^f_x$ and $\bar{\chi}^f_x$ are the staggered fermion fields with flavour $f = u, d, s$. On the configurations of our Monte-Carlo sample, we compute correlation functions (2) neglecting disconnected diagrams similarly to Ref. [21–23]. The staggered fermion correlator (2) corresponds to two different operators for the even $\tau = 2n \times a$ and odd $\tau = (2n + 1) \times a$ time slices, where a is the lattice spacing, while n is an integer that takes value from 0 to the half dimensionless temporal extension $N_t/2 - 1$, since the inverse temperature is $\beta_T = N_t a$. In the Dirac spinor basis, $C_{ij}(\tau)$ reads

$$C^{\mathrm{e,\,o}}_{ij}(\tau) = \sum_{\vec{x}} \left(\langle A_i(x)A_j(0)\rangle - s^{\mathrm{e,\,o}}\langle B_i(x)B_j(0)\rangle\right), \tag{4}$$

where $s^{\mathrm{e,\,o}} = (-1)^\tau$ is the timeslice parity and

$$A_i = e\sum_f q_f \bar{\psi}^f \gamma_i \psi^f, \quad B_i = e\sum_f q_f \bar{\psi}^f \gamma_5\gamma_4\gamma_i\psi^f,$$

where ψ^f is the f flavoured Dirac spinor. The operator A_i corresponds to the continuum electromagnetic current, whereas B_i is a spurious contribution to be removed.
Now, let us recall that the current-current Euclidean correlators C^{eo}_{ij}, both for even and odd slices, are related to the corresponding spectral functions $\rho^{\mathrm{e,\,o}}_{ij}(\omega)$ by

$$C^{\mathrm{e,\,o}}_{ij}(\tau) = \int_0^\infty \frac{d\omega}{\pi} K(\tau,\omega)\rho^{\mathrm{e,\,o}}_{ij}(\omega), \tag{5}$$

where $K(\tau,\omega) = \frac{\cosh\omega\,(\tau-\beta/2)}{\sinh\omega\,\beta/2}$. The crucial point, here, is that if we are able to extract the spectral densities $\rho^{\mathrm{e,\,o}}_{ij}(\omega)$ from the lattice correlators, then we can compute the electromagnetic conductivity σ_{ij} using the Kubo formulas

$$\frac{\sigma_{ij}}{T} = \frac{1}{2T}\lim_{\omega\to 0}\frac{1}{\omega}\left(\rho^{\mathrm{e}}_{ij}(\omega) + \rho^{\mathrm{o}}_{ij}(\omega)\right). \tag{6}$$

The contribution from $\langle B_i(\tau)B_j(0)\rangle$ cancels out in the sum $\rho^e_{ij} + \rho^o_{ij}$ and, in the continuum limit, the electromagnetic conductivity is reproduced. In the following paragraph, we discuss the inversion strategies applied in our analysis to extract the spectral functions from the corresponding lattice correlation functions.

4. Inversion smearing methods

Given the correlation functions $C^{\mathrm{e,\,o}}_{ij}(\tau)$, one needs to invert the integral equation (5) to obtain the spectral functions $\rho^{\mathrm{e,\,o}}_{ij}(\omega)$, in order to find the conductivity using (6). Let us rewrite Eq. (5) as

$$C(\tau) = \int_0^{+\infty} \frac{d\omega}{\pi}\frac{\rho(\omega)}{f(\omega)}K'(\tau,\omega), \tag{7}$$

where we redefined the basis functions as

$$K'(\tau,\omega) = \frac{\cosh\omega\ (\tau-\beta/2)}{\sinh\omega\ \beta/2}f(\omega)$$

in order to introduce the arbitrary function $f(\omega)$. We can make an estimate of the spectral function as

$$\bar{\rho}(\bar{\omega}) = \pi f(\bar{\omega})\sum_{\tau=\tau_{min}}^{\tau_{max}} q_i(\bar{\omega})C(\tau_i). \tag{8}$$

where q_i are coefficients that have to be fixed. The advantage of the rearrangement in Eq. (7) is that we can choose $f(\omega) = \omega$ and $\bar{\omega} = 0$, so that we can directly extract from the correlators the ratios $\rho_{ij}^{e,o}(\omega)/\omega$ in the limit $\omega \to 0$. This is exactly what we need to compute the conductivity using Eq. (6). Thus, in our analysis $\bar{\omega} = 0$. The relation between the estimator $\bar{\rho}(\bar{\omega})$ and the spectral function $\rho(\omega)$ is

$$\bar{\rho}(\bar{\omega}) = f(\bar{\omega}) \int_0^\infty d\omega \, \Delta(\bar{\omega}, \omega) \frac{\rho(\omega)}{f(\omega)}, \tag{9}$$

where $\Delta(\bar{\omega}, \omega) = \sum_{\tau=\tau_{min}}^{\tau_{max}} q(\bar{\omega}, \tau) K(\omega, \tau)$ is the resolution function. Notice that the calculation is hindered by large ultraviolet (UV) contribution of $\rho(\omega)$. For the conductivity the UV contribution scales as $\rho \propto \omega^2$ and the study carried out in Ref. [25] shows that it corresponds to $\sim 20 - 30\,\%$ of the total signal at $\bar{\omega} = 0$. One could subtract the UV contribution from the correlation function (4) (see Ref. [25] for details). However, this approach leads to large uncertainties. In this work, we solve this issue by considering the change ΔC of correlation functions at different values of the parameters of the analysis, instead of the simple correlation functions C. We clarify this point in the following paragraphs when we enter in the details of the specific considered physical situations.

To find the coefficients q_i we applied a recently proposed modified version of the Backus-Gilbert method [27]. Here, the quantities q_i are fixed as the ones that minimize the deviation between the smearing function $\Delta(\bar{\omega}, \omega)$ appearing in Eq. (9) and a reasonable target function. Then, the minimization is regularized by means of a regularization parameter λ. This approach results to be more stable and it also allows us to have a clearer estimate of the systematic uncertainty related to the final result. However, let us recall here that, in the case of staggered fermions, one has two branches of lattice data: even and odd. So we apply separately the approach to the two branches and then we sum them in Eq. (6). In this work, in some cases, we use lattices that return correlation functions having also just three independent values of the Euclidean time (for lattices with $N_t = 12$). Using these few independent terms, it is difficult to build the gaussian target function proposed in [27]. For this reason, we choose the target function as

$$\delta_0(\omega) = \delta_0(\omega, \bar{\omega} = 0) = \frac{1}{(\sigma\pi/2)^2} \frac{\omega}{\sinh(\omega/\sigma)}. \tag{10}$$

The advantage of using this function stems from the fact that at $\sigma = 2\,T$ it coincides with the thermal kernel at $\tau = \beta/2$, namely $\delta_0(\omega) \sim \omega K(\beta/2, \omega)$ (see formula (7)). This implies that, at $\sigma = 2\,T$, only one point is needed to exactly reproduce $\delta_0(\omega)$. At $\sigma \neq 2\,T$, more points are needed, but not as many as for the gaussian target function in [27].

Let us now describe how we fixed the value of the σ parameter. We consider the relative deviation r without regularization, namely $\lambda = 0$, as a function of the smearing parameter σ/T. Then, we impose the requirement that the relative deviation at the peak position $\omega = \bar{\omega}$ is smaller than 5 %. The resulting intersection gives the value of σ.

To fix the value of the λ parameter we study the behaviour of the output spectral function as a function of the λ parameter. Then, we choose λ approximately in correspondence of the point, starting from larger values of λ, at which the spectral function reaches a stabilization. This plateau has a lower limit fixed by the fact that the uncertainties must be still reliable. Differently, the upper limit is fixed by the physical range of the quantity we are studying. Indeed, in a real calculation, the resolution function has a peak of finite width of some T. Thus, the estimator $\bar{\rho}(\bar{\omega})$ is an average of the spectral function over such a region around $\bar{\omega}$. Note that we can reliably reconstruct $\rho(\omega = 0)$ if the resolution function $\delta(\bar{\omega} = 0, \omega)$ is narrower than the characteristic variation scale of $\rho(\omega)$. Correlation functions of the electromagnetic currents are well described by either the ansatz combining the transport peak at small frequencies and UV contribution at large frequencies [22–24] or by the AdS/CFT spectral function [24]. Thus, we have to take temperature interval such that the widths of $\delta(\bar{\omega} = 0, \omega)$ are close to or smaller than the variation scale of $\rho(\omega)$ obtained in [22–24]. We fix λ_{max} such that the width is $\sim 4T$. This choice allows us to obtain reliable results for the conductivity extracted from such

spectral functions. Finally, after the determination of the λ parameter and the corresponding coefficients q_i, one can obtain the estimate of the observable. The related systematic uncertainties are computed as proposed in Ref. [27], while the statistical uncertainties are evaluated by using a bootstrap sampling.

5. Conductivity at finite baryon density

It is known that QGP created in heavy-ion collision experiments has nonzero baryon density. It is believed to be rather small for LHC and RHIC experiments while FAIR and NICA are designed to generate large baryon densities. One can expect that a non vanishing density leads to the appearance of additional fermion states in QGP, which might play an important role in the charge transport phenomena. Thus, it is important to study how a nonzero baryon density influences the electromagnetic conductivity of QGP. Several phenomenological studies investigated transport properties in this regime [29–32]. Lattice QCD study where the electromagnetic conductivity dependence on the baryon density was considered, are in general very difficult. Partially, this is due to the notorious sign problem of lattice simulations at finite baryon density; indeed, in QCD-like theories without the sign problem, the conductivity can be studied through lattice simulations at finite baryon density [33].

Here, we conduct the lattice study within real QCD, based on [1], considering in particular the theory with $N_f = 2 + 1$ dynamical quarks at the physical point. To overcome the sign problem, simulations are carried out using an imaginary baryon chemical potential; then, the obtained results are analytically continued to real values of the chemical potential. We consider chemical potentials μ_f ($f = u, d, s$), in a setup for which $\mu_u = \mu_d = \mu_B/3$, $\mu_s = 0$; that does not reproduce the exact condition present in heavy ion collisions, which corresponds to strangeness neutrality, but are nevertheless quite close to it. We adopt the standard exponentiated implementation of the chemical potentials [34, 35] taking the staggered fermion matrix appearing in Eq. (1) as

$$\begin{aligned} M^f_{\rm st}(U,\mu_f)_{x,y} &= am_f\delta_{x,y} + \sum_{\nu=1}^{4}\frac{\eta_{x;\nu}}{2}\Big[e^{a\mu_f\delta_{\nu,4}}U^{(2)}_{x;\nu}\delta_{x,y-\hat{\nu}} \\ &- e^{-a\mu_f\delta_{\nu,4}}U^{(2)\dagger}_{x-\hat{\nu};\nu}\delta_{x,y+\hat{\nu}}\Big], \end{aligned} \tag{11}$$

where $\eta_{x;\nu} = (-1)^{x_1+..x_{\nu-1}}$ are the staggered phases, and $U^{(2)}_{x;\nu}$ are two-times stout-smeared links, with isotropic smearing parameter $\rho = 0.15$ [36]. We consider two temperature values, namely $T = 200$ and 250 MeV; most simulations are carried out on a 12×48^3 lattice, with spacings $a = 0.0820$ fm and $a = 0.0657$ fm, correspondingly. To study the cutoff dependence, we also consider a 10×48^3 lattice with $a = 0.0988$ fm and $a = 0.0788$ fm. To avoid the sign problem, we carry out the simulations using an imaginary baryon chemical potential, $\mu_B = i\mu_I$, with values $\mu_I/(3\pi T) = 0.000$, 0.140, 0.200, 0.245 and 0.285 for all UV cutoffs and lattice sizes.

We choose bare parameters in order to stay on a line of constant physics with physical quark masses. In particular, we adopt the values reported in Refs. [37–39], either directly or by interpolation. We use up to $O(100)$ decorrelated gauge configurations for each simulation point. They are obtained using the Rational Hybrid Monte-Carlo algorithm [40–42]. In Table 1 we provide a sketch of simulations parameters.

As mentioned above, the calculation is hindered by large ultraviolet (UV) contribution of $\rho(\omega)$. Thus, in this case, instead of the correlation functions $C^{\rm e,\,o}_{\mu_I}$, we consider the differences $\Delta C^{\rm e,\,o} = C^{\rm e,\,o}_{\mu_I} - C^{\rm e,\,o}_{\mu_I=0}$. Since for the chosen values of the lattice spacing the UV regime starts at $\omega_0 \sim 2$ GeV [25], we note that $\mu_I \ll \omega$ for all frequencies in the UV regime and for our values of the imaginary baryon chemical potential. Thus, one can consider the UV spectral function independent of the imaginary baryon chemical potential and assume that the differences $\Delta C^{\rm e,\,o}$ do not contain significant UV artefacts. The results for $\Delta C^{\rm e,\,o}$ also turn out to be more accurate since the UV–estimation uncertainty is absent in this case.

To sum up, in our study first of all we measure the lattice correlation functions $C^{\rm e,\,o}_{ij}(\tau)$ (4). Then, we compute the differences $\Delta C^{\rm e,\,o}_{ij}$ from which we extract the estimators $\Delta\bar{\rho}^{\rm e,\,o}_{ij}(\bar{\omega})/\bar{\omega}$ at $\bar{\omega} = 0$ using the improved BG inversion method. Finally, using Eq. (6), we calculate the electromagnetic conductivity $\Delta\sigma = \sigma_{\mu_I} - \sigma_{\mu_I=0}$.

a, fm	L_s	N_t	T, MeV	$m_l a$	$m_s a$	$\mu_I/3\pi T$
0.0988	48	10	200	0.00140	0.03940	0.0, 0.14, 0.20, 0.245, 0.285
0.0788	48	10	250	0.00112	0.03151	0.0, 0.14, 0.20, 0.245, 0.285
0.0820	48	12	200	0.00117	0.03287	0.0, 0.14, 0.20, 0.245, 0.285
0.0657	48	12	250	0.00092	0.02581	0.0, 0.14, 0.20, 0.245, 0.285

Table 1: *Parameters used in the numerical simulations.*

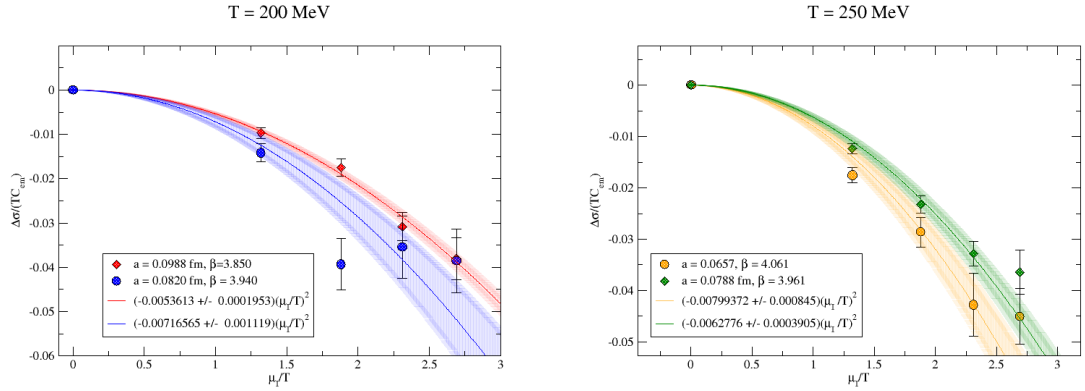

Figure 1: *The Figures show the results of the change of the electromagnetic conductivity due to non-zero imaginary baryon chemical potential $\Delta\sigma = \sigma_{\mu_I} - \sigma_{\mu_I=0}$ as a function of μ_I/T normalized to TC_{em}, obtained by the modified Backus-Gilbert using the plateau technique. The calculations are carried out for $T = 200MeV$ (left panel) and $T = 250MeV$ (right panel).*

The variation of the electromagnetic conductivity due to a non-zero imaginary baryon chemical potential, $\Delta\sigma = \sigma_{\mu_I} - \sigma_{\mu_I=0}$, normalized to TC_{em} is shown as a function of μ_I in Fig. 1. The obtained results are well described by the quadratic polynomial

$$\frac{\Delta\sigma}{TC_{em}} = -c(T)\left(\frac{\mu_I}{T}\right)^2, \tag{12}$$

which, after analytical continuation to real chemical potentials, becomes

$$\frac{\Delta\sigma}{TC_{em}} = c(T)\left(\frac{\mu_B}{T}\right)^2. \tag{13}$$

The values of the coefficients $c(T)$ are shown in Table 2. Notice that the coefficients for all lattice parameters are positive. Thus, we conclude that a non-zero real baryon chemical potential enhances the electromagnetic conductivity. This can be understood as follows: a nonzero baryon density introduces additional fermion states into the QGP, which participate in the charge transport, leading to a conductivity enhancement.

6. Conductivity in presence of strong magnetic field

The investigation of QCD properties in a magnetic background field has been the subject of various studies in the last few years, see, e.g., Refs. [43–45] for recent reviews. Part of the interest is directly related

a, fm	T, MeV	c(T)
0.0988	200	0.0125(11)
0.0788	250	0.0095(6)
0.0820	200	0.0109(17)
0.0657	250	0.0165(5)

Table 2: *The parameter $c(T)$ in the quadratic fit obtained within modified Backus-Gilbert method.*

to phenomenology, since strong background fields are expected in non-central heavy ion collisions. A central aspect for the understanding of these collisions is the Chiral Magnetic Effect (CME), a well known anomaly-based phenomenon which can be realized in different systems with relativistic fermionic degrees of freedom [46–48]. The CME is the generation of a non-dissipative electric current along the external magnetic field in systems with a net imbalance between the number of right-handed and left-handed fermions or nonzero chiral density. The nonzero chiral density should be generated in order to experimentally observe the CME. In heavy-ion experiments the chiral density might be generated due to sphaleron transitions in the quark-gluon plasma (QGP), namely the deconfined phase of QCD. A possible way to generate the chiral density and to observe the CME is to apply parallel electric and magnetic fields. In this case the chiral anomaly generates the imbalance between the right-handed and left-handed fermions which leads to the CME which manifests itself through the rise of electric conductivity along the magnetic field. This CME current has already been observed experimentally in condensed matter systems [49–51]. Similarly to condensed matter systems, the latter mechanism can be realized in heavy-ion experiments, where colliding ions create hot QGP with deconfined relativistic quarks. In addition, in non-central collisions the QGP is affected by huge magnetic fields generated by the motion of colliding heavy ions [52]. As a result the electromagnetic (e.m.) conductivity of QGP along the magnetic field might be significantly enhanced. A first lattice study of the e.m. conductivity of QGP in external magnetic field with $N_f = 2 + 1$ dynamical staggered fermions has been performed in [25].

Here, our analysis is carried out on the same configurations used by authors of [53] to study QCD phase diagram in the $T - eB$ plane. Their results suggest a crossover transition in correspondence of $eB = 4GeV^2$ at a temperature $\sim 98MeV$ and a first order transition in correspondence of $eB = 9GeV^2$ at a temperature $\sim 63MeV$. Since the magnetic field is directed along the z-direction, the symmetry of the space is broken. Thus, we study separately the parallel and the perpendicular component of the conductivity. As described in [25], the total conductivity of the system is the sum of the Ohmic and the CME conductivities. In the perpendicular direction the CME component is zero, since there is no magnetic field. It remains only the Ohmic component which gives the magnetoresistance effect. Differently, in the parallel direction the CME component is a raising function of the magnetic field. Thus, the observation of a parallel conductivity raising with the magnetic field can be a manifestation of the CME. The extraction of the conductivity is performed using the improved Backus-Gilbert method with the procedure described in the previous Sections. Also in this case, we consider the difference $\Delta C^{e,o} = C_{eB} - C_{eB=0}$. In Figure 2 we show the results for the perpendicular conductivity normalized to TC_{em}, in the only case in which we obtain reliable results, as a function of the temperature. Unfortunately our data for other parameters are affected by large errors ($\sim 100\%$), that together with the fact that the signal is small make the method unstable, making impossible the λ-tuning in the physical range and producing unreliable results. The magnetic field has the clear effect of decreasing the conductivity. Indeed, the change of the conductivity $\Delta\sigma = \Delta\sigma_{eB} - \Delta\sigma_{eB=0}$ is negative. We interpret this as the magnetoresistance effect. For higher temperatures this difference becomes smaller in modulus. This is reasonably due to the increased thermal activity. Around $T = 98MeV$ we have the transition. However in this region the large uncertainties forbid to make conclusions.

For the parallel case, always normalized to TC_{em}, the signal is stronger and the errors are in general smaller ($\sim 10\%$). Consequently, the modified BG method is more stable within the physical range. It is clearly

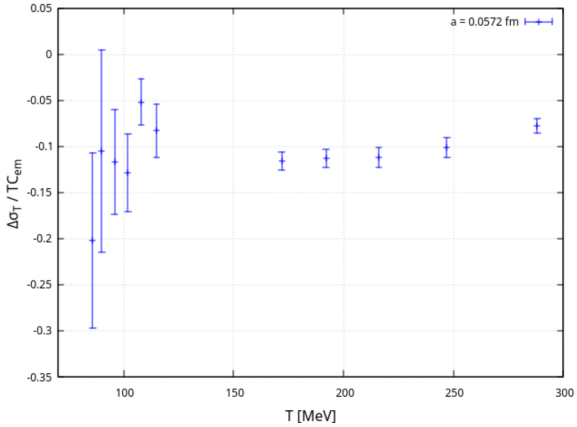

Figure 2: *Perpendicular electromagnetic conductivity due to the magnetic field as a function of the temperature $T = 1/N_t a$ for $eB = 4GeV^2$ and $a = 0.0572\,fm$.*

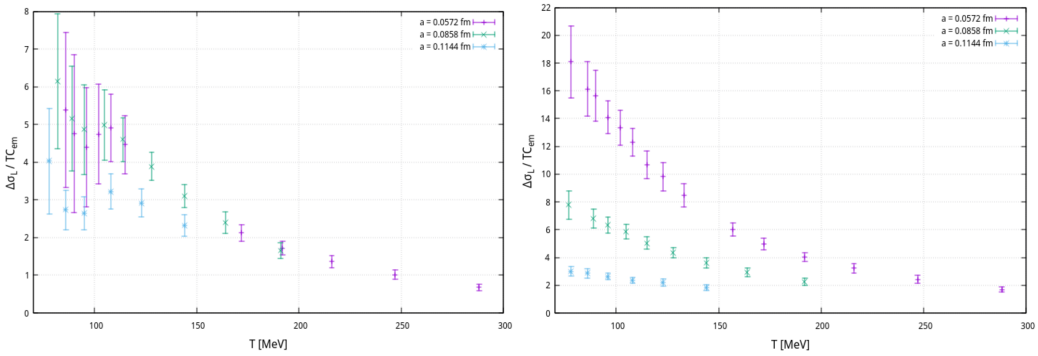

Figure 3: *Parallel electromagnetic conductivity due to the magnetic field as a function of T for different magnetic fields and lattice spacings. Left : $eB = 4\ GeV^2$. Right : $eB = 9\ GeV^2$.*

observed an important increase of the conductivity for both the values of the magnetic field. This is the manifestation of the CME in QGP on the lattice. In the case of $eB = 9GeV^2$, all the considered temperatures are larger than the deconfinement one. Thus, all the points are in the deconfined region of the phase diagram. Differently, as in the perpendicular case, for $eB = 4GeV^2$ we have points also around the deconfinement point. However, also in this case the errors forbid us to draw any reliable conclusion. Further investigations are needed.

7. Conclusion and Outlook

The conductivity of a physical system is directly related to the spectral function of the current-current electromagnetic correlation functions via the Kubo formulas. The extraction of the conductivity from the euclidean correlation functions is an inverse problem that we solve using the modified BG approach [27]. We considered the study of the conductivity of the QGP in two cases relevant for the phenomenology of the heavy ion collisions. In the first case, we analysed the effect of a non-zero baryon density on the conductivity. Our results indicate that the baryon density has a clear effect on the conductivity, namely it enhances its magnitude. In the second application, we considered the presence of large magnetic fields, namely $eB = \{4, 9\}\ GeV^2$, directed along the z axis. Using the same techniques, we studied separately the parallel and the perpendicular conductivity with respect the direction of the magnetic field. In the case of the perpendicular component, we observed a decreasing of the conductivity and then a manifestation of the magnetoresistance. Differently, the

parallel component increases with the magnetic field. We interpret this as a manifestation of the CME.
Numerous questions are still open and claim for further investigations. From a methodological point of view, we plan to improve the approaches that we used to solve inverse problems. In this work we used the modified Backus-Gilbert approach proposed in [27]. This method is surely more stable than the original one. However many aspects remain to be clarified. First of all, there should be a better clarification of the relation between the two terms entering in the expression of the functional, defined in Eq (26) of [27], that we minimize to extract the coefficients. Even if they have the same dimensions, the comparison of the two functionals still remains not completely meaningful from a mathematical point of view. This problem is directly related to the tuning of the λ parameter. This regularization parameter is not fixed by the method and the proposal, made in [27], of fixing it as the maximum value assumed by the function $W(\lambda)$ remains not effective, since this value often corresponds to a point which is far from the stabilization region of the output as a function of λ. Looking at a plateau of the output quantity as a function of λ seems to be more reasonable. However, the choice of λ still remains too subjective, since we don't have a clear rule that can be applied to fix it. This implies that the fixing of its value is case dependent. For this reason, it's not possible for the moment to automatize the analysis making it meaningful and efficient in every situation. Another important point to be improved is the evaluation of the systematic uncertainties. The recent modified BG approach [27] surely improved its definition making its evaluation more clear. However, it is still not a definition that can be considered definitive. A further investigation is necessary.
From a physical point of view, the present work can be extended in various directions, which however require considerable additional computational efforts. For both physical applications, we would like to explore a broader range of lattice spacing, especially finer ones, in order to better assess the impact of using different resolution functions and also to perform a continuum limit extrapolation. Including simulations with more time slices would allow us to perform the inversion using narrower resolution functions. This would be crucial to obtain an observable which better approximate the physical quantity. In the case of the conductivity in presence of baryon density, we plan to explore a wider temperature range. Together with a reduction of statistical and systematic uncertainties, it could permit to make a more definite assessment on the T dependence of the coefficients $c(T)$. We also plan to refine the setup of quark chemical potentials, in order to be closer to the phenomenological conditions reproduced in heavy ion collisions. In the case of the conductivity in presence of strong magnetic field, the study of the temperature dependence of the conductivity in the parallel direction has to be better investigated. Indeed, especially for large values of the temperature, the conductivities in the parallel direction seem to manifest a common behaviour. We plan to study this dependence and investigate which could be its physical origin. Finally, it would also be very interesting to investigate the conductivity for $eB = 9\ GeV^2$ around the deconfinement temperature where in [53] the authors guess a first order transition that could be observed as a jump of the conductivity.

References

[1] Astrakhantsev, N. et al., PoS **LATTICE2021** (2022) 119.
[2] Tuchin, K., Adv. High Energy Phys. **2013** (2013) 490495.
[3] McLerran, L. D. and Toimela, T., Phys. Rev. D **31** (1985) 545.
[4] Harutyunyan, A., Rischke, D. H., and Sedrakian, A., Phys. Rev. D **95** (2017) 114021.
[5] Singha, P., Abhishek, A., Kadam, G., Ghosh, S., and Mishra, H., J. Phys. G **46** (2019) 015201.
[6] Saha, K., Ghosh, S., Upadhaya, S., and Maity, S., Phys. Rev. D **97** (2018) 116020.
[7] Marty, R., Bratkovskaya, E., Cassing, W., Aichelin, J., and Berrehrah, H., Phys. Rev. C **88** (2013) 045204.
[8] Ghosh, S., Bandyopadhyay, A., Farias, R. L. S., Dey, J., and Krein, G. a., Phys. Rev. D **102** (2020) 114015.
[9] Soloveva, O., Fuseau, D., Aichelin, J., and Bratkovskaya, E., Phys. Rev. C **103** (2021) 054901.

[10] Arnold, P. B., Moore, G. D., and Yaffe, L. G., JHEP **11** (2000) 001.
[11] Arnold, P. B., Moore, G. D., and Yaffe, L. G., JHEP **05** (2003) 051.
[12] Greif, M., Bouras, I., Greiner, C., and Xu, Z., Phys. Rev. D **90** (2014) 094014.
[13] Berrehrah, H., Bratkovskaya, E., Steinert, T., and Cassing, W., Int. J. Mod. Phys. E **25** (2016) 1642003.
[14] Fotakis, J. A., Soloveva, O., Greiner, C., Kaczmarek, O., and Bratkovskaya, E., (2021).
[15] Rose, J. B., Torres-Rincon, J. M., Schäfer, A., Oliinychenko, D. R., and Petersen, H., Phys. Rev. C **97** (2018) 055204.
[16] Greif, M., Greiner, C., and Denicol, G. S., Phys. Rev. D **93** (2016) 096012, [Erratum: Phys.Rev.D 96, 059902 (2017)].
[17] Fernandez-Fraile, D. and Gomez Nicola, A., Phys. Rev. D **73** (2006) 045025.
[18] Kim, K.-Y., Sin, S.-J., and Zahed, I., JHEP **07** (2008) 096.
[19] Fukushima, K. and Okutsu, A., (2021).
[20] Ding, H. T. et al., Phys. Rev. D **83** (2011) 034504.
[21] Amato, A. et al., Phys. Rev. Lett. **111** (2013) 172001.
[22] Aarts, G. et al., JHEP **02** (2015) 186.
[23] Brandt, B. B., Francis, A., Jäger, B., and Meyer, H. B., Phys. Rev. D **93** (2016) 054510.
[24] Ding, H.-T., Kaczmarek, O., and Meyer, F., Phys. Rev. D **94** (2016) 034504.
[25] Astrakhantsev, N. et al., Phys. Rev. D **102** (2020) 054516.
[26] Aarts, G. and Nikolaev, A., Eur. Phys. J. A **57** (2021) 118.
[27] Hansen, M., Lupo, A., and Tantalo, N., Physical Review D **99** (2019).
[28] Curci, G., Menotti, P., and Paffuti, G., Phys. Lett. B **130** (1983) 205, [Erratum: Phys.Lett.B 135, 516 (1984)].
[29] Steinert, T. and Cassing, W., Phys. Rev. C **89** (2014) 035203.
[30] Srivastava, P. K., Thakur, L., and Patra, B. K., Phys. Rev. C **91** (2015) 044903.
[31] Tripolt, R.-A., Jung, C., Tanji, N., von Smekal, L., and Wambach, J., Nucl. Phys. A **982** (2019) 775.
[32] Soloveva, O., Moreau, P., and Bratkovskaya, E., Phys. Rev. C **101** (2020) 045203.
[33] Buividovich, P. V., Smith, D., and von Smekal, L., Phys. Rev. D **102** (2020) 094510.
[34] Hasenfratz, P. and Karsch, F., Phys. Lett. B **125** (1983) 308.
[35] Gavai, R. V., Phys. Rev. D **32** (1985) 519.
[36] Morningstar, C. and Peardon, M. J., Phys. Rev. D **69** (2004) 054501.
[37] Aoki, Y. et al., JHEP **06** (2009) 088.
[38] Borsanyi, S. et al., JHEP **11** (2010) 077.
[39] Borsanyi, S. et al., Phys. Lett. B **730** (2014) 99.
[40] Clark, M. A., Kennedy, A. D., and Sroczynski, Z., Nucl. Phys. B Proc. Suppl. **140** (2005) 835.
[41] Clark, M. A. and Kennedy, A. D., Phys. Rev. Lett. **98** (2007) 051601.
[42] Clark, M. A. and Kennedy, A. D., Phys. Rev. D **75** (2007) 011502.
[43] Kharzeev, D. E., Landsteiner, K., Schmitt, A., and Yee, H.-U., Lect. Notes Phys. **871** (2013) 1.
[44] Andersen, J. O., Naylor, W. R., and Tranberg, A., Rev. Mod. Phys. **88** (2016) 025001.
[45] Miransky, V. A. and Shovkovy, I. A., Phys. Rept. **576** (2015) 1.
[46] Fukushima, K., Kharzeev, D. E., and Warringa, H. J., Phys. Rev. D **78** (2008) 074033.
[47] Kharzeev, D. E., Prog. Part. Nucl. Phys. **75** (2014) 133.
[48] Kharzeev, D. E., Liao, J., Voloshin, S. A., and Wang, G., Prog. Part. Nucl. Phys. **88** (2016) 1.
[49] Li, Q. et al., Nature Phys. **12** (2016) 550.
[50] Li, H., H. H. L. H. e. a.
[51] Li, CZ., W. L. L. H. e. a., Nat Commun. **6 10137** (2015).
[52] Kharzeev, D. E., McLerran, L. D., and Warringa, H. J., Nucl. Phys. A **803** (2008) 227.
[53] D'Elia, M., Maio, L., Sanfilippo, F., and Stanzione, A., Phys. Rev. D **105** (2022) 034511.